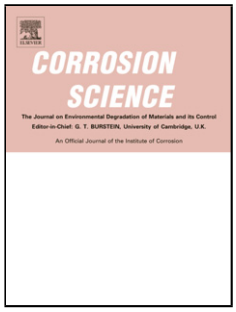

Title: Anomalous oxidation of Fe-Si alloys under a low oxygen pressure at 800 °C

Author: L.L. Liu Q.Q. Guo S. Liu C.S. Ni Y. Niu

PII: S0010-938X(15)00250-4
DOI: http://dx.doi.org/doi:10.1016/j.corsci.2015.05.055
Reference: CS 6342

To appear in:

Received date: 19-12-2014
Revised date: 22-5-2015
Accepted date: 23-5-2015

Please cite this article as: L.L. Liu, Q.Q. Guo, S. Liu, C.S. Ni, Y. Niu, Anomalous oxidation of Fe-Si alloys under a low oxygen pressure at 800<ce:hsp sp=Ö.25Ï/>^{circ}C, *Corrosion Science* (2015), http://dx.doi.org/10.1016/j.corsci.2015.05.055

Anomalous oxidation of Fe-Si alloys under a low oxygen pressure at 800 °C

L.L. Liu [a, b], Q.Q. Guo[a], S. Liu[a], C. S. Ni[c], Y. Niu[a*]

[a] Institute of Metal Research, Chinese Academy of Sciences, Wencui Road 62, 110016 Shenyang (China)

[b] Live-line Working Center, State Grid Hunan Electric Power Company, 410000 Changsha (China)

[c] School of Chemistry, University of St Andrews, Fife KY16 9ST (Scotland)

[*] Corresponding author. E-mail address: yniu@imr.ac.cn

Abstract: The oxidation of three Fe-xSi alloys (x=5, 9, 13 at.%) under 10^{-20} atm O_2 at 800 °C formed in all cases SiO_2 layers. For Fe-5Si this layer broke down and healed up periodically forming an anomalous internal oxidation zone with spherical and net-shaped SiO_2 particles. The SiO_2 layer formed on the other two alloys spalled off due to the growth and thermal stress accumulated. The critical silicon content needed for its external oxidation on Fe-Si alloys calculated according to an extension of Wagner's theory under the present experimental conditions is significantly smaller than the experimental results.

KEY WORDS: A iron, B SEM, C internal oxidation, C amorphous structures

1. Introduction

Silicon is one of the most important alloying elements in commercial steels used in the manufacture of automobile bodies and frames and in the cores of motors and transformers. However, the oxidation properties of silicon steels seriously affected their application. Up to now, the oxidation of Fe-Si alloys with different silicon contents has been the subject of many investigations in different atmospheres, including air [1-6], pure O_2 [7-9], CO_2+CO [10-12], air+H_2O [4,13], CO+H_2+H_2O [14,15], H_2+H_2O [16,17], CO_2+H_2O [18,19], H_2+N_2+H_2O [20,21]. In these studies, the internal oxidation of silicon in Fe-Si alloys has been observed both in the presence [2,5,7,13,16-20] and in the absence [14,15,21] of external iron oxides. In the latter case, when the silicon content was less than 2 at.%, the

shape of the SiO_2 particles was spherical [21], while for larger silicon contents, for example 5 at.% and 9 at.%, dendritic SiO_2 particles started to appear and were associated with the appearance of a thin continuous SiO_2 layer at the interface between the internal oxidation zone (ioz), and the base alloy [14]. This structure of the ioz, differing from the classical type which does not involve the presence of a nearly continuous layer of internal oxide at the interface between the ioz and the alloy but only a direct transition to an alloy matrix free from oxide particles, is named here as an anomalous ioz. However, the formation mechanism of this peculiar internal oxidation zone was not considered in details in the previous paper [14]. The present study examines the oxidation behavior of three Fe-Si alloys with rather high silicon contents under an oxygen pressure below the decomposition of the iron oxides. The critical silicon content required for the exclusive external oxidation of silicon is calculated and compared with the experimental results. The scale evolution is presented for different reaction times and silicon contents: in particular, the anomalous type of internal oxidation has been observed for the two more dilute alloys.

2. Experimental

Three Fe-Si alloys with nominal silicon contents of 5, 9 and 13 at.% (Fe-5Si, Fe-9Si and Fe-13Si, respectively) were prepared by repeated melting by vacuum induction mixtures of appropriate amounts of the two pure elements (99.8% Fe and 99.99% Si). The alloy ingots were subsequently annealed in 1 atm argon at 1000 ^{o}C for 36 h to remove the residual mechanical stresses and achieve a better alloy equilibration. The actual composition of the alloys, measured by inductively coupled plasma (ICP) spectrometry, is shown in Table 1. In agreement with the Fe-Si phase diagram, Fe-5Si and Fe-9Si are single-phase α, while Fe-13Si is single-phase α_1 [22]. The average grain sizes of the three alloys were 1.59 (Fe-5Si), 1.12 (Fe-9Si) and 0.506 mm (Fe-13Si) calculated according to the procedure described in GB/T 6394-2002.

Specimens with a size of 10×8×1.5 mm were cut from the ingots using a line saw and a 1 mm hole was drilled near one edge. All the specimens were mechanically abraded on successively finer abrasive papers down to 2000 grit and finally cleaned with water, acetone and ethanol and dried immediately before each test. Prior to the experiment, each specimen

was first suspended in the reaction chamber by quartz fibers and a Pt wire. The reaction tube was then flushed with the gas mixture from below with a counter flow of nitrogen from the top for about half an hour. A Pt gauze was placed below the sample at a distance of less than 1 cm in the hot zone to facilitate reaching equilibrium. After reaching the reaction temperature, the vertical furnace was raised to locate the specimen in the hot zone. The mass changes of the specimens were continuously recorded with a microbalance Setaram B-92. The mass of each specimen was also measured with an electronic balance before and after oxidation as a check of the recorded mass changes. The oxidized samples were examined by SEM (FEI INSPECT F 50, USA) attached with EDS (OXFORD X-Max, UK) and by X-ray diffraction (Panalytical X' Pert PRO, Holland). In addition, the oxidized samples prepared for observing the cross sections were ground down mechanically by 5000 emery paper after being mounted by resin and then polished by emery and diamond pastes. By equilibration at 800°C the reacting gas, composed of 13.2 vol.% CO_2 balance H_2, provided an oxygen pressure of 10^{-20} atm. To identify the structure of the internal oxide particles in three dimensions, some samples, mounted in a direction parallel or perpendicular to the large face (10×8 mm), were etched with a $CuSO_4$ solution to remove iron from the internal oxidation zone to different degrees.

3. Results

3.1 Kinetic results

Parabolic plots of the kinetic curves obtained for the three alloys oxidized under the present conditions are shown in Fig. 1. The mass gains of these alloys after a fixed reaction time decreased with an increase of the silicon content, an effect which was particularly large in shifting from Fe-5Si to Fe-9Si. The kinetic curves did not follow the conventional parabolic rate law, which involves linear parabolic plots, and were generally rather irregular, presenting values of the instantaneous slope of the parabolic plot, denoted as instantaneous parabolic rate parameter (iprp), changing with time. In particular, the iprp of Fe-5Si decreased continuously with time from an initial value of $1.1\text{x}10^{-11}$ $g^2cm^{-4}s^{-1}$ to a limiting value of $6.5\text{x}10^{-14}$ $g^2cm^{-4}s^{-1}$, reached after about 10 h, which then remained constant up to the end of the experiment.

The oxidation of Fe-9Si showed a continuous increase of the iprp with time and followed approximately two parabolic stages with parabolic rate constant k_p of the first stage, lasting from 2 to 17 h, equal to to $4.9x10^{-14}$, while that of the second stage, lasting from 18 to 24 h, equal to $9.9x10^{-14}$ $g^2cm^{-4}s^{-1}$. Conversely, the oxidation of Fe-13Si showed a continuous decrease of the iprp with time and was more irregular (Fig. 1b), showing a first faster stage of about 2 h with a $k_p = 2.3x10^{-13}$ $g^2cm^{-4}s^{-1}$, followed by a second approximately parabolic stage lasting from 4 to 24 h with a $k_p = 1.7x10^{-15}$ $g^2cm^{-4}s^{-1}$.

3.2 Scale structure and composition

Cross sections of Fe-5Si oxidized for 4 different times (1.5, 4, 18 and 24 h) are shown in Fig. 2. In all cases iron oxides did not form, as shown in Fig. 3, while an SiO_2 layer containing some iron (the oxide layer is too thin to obtain an accurate analysis) formed at the front of the internal oxidation zone; this layer was discontinuous for samples oxidized for 1.5 and 4 h (Figs. 2a-2b) but became continuous after longer reaction times (Figs. 2c-2e). Actually, the structure of the zone formed between the SiO_2 layer and the gas phase was different from the classical model of internal oxidation [23,24] for different reasons, thus presenting an anomalous internal oxidation zone. In fact, the SiO_2 particles in the ioz were not only spherical, with radii ranging from tens to several hundreds of nm, but also vermicular. In addition, the content of SiO_2 particles with vermicular shape increased with an increase of the oxidation time (Figs. 2a-2e). Finally and most importantly, a continuous layer of SiO_2 tended to form at the base of the ioz and in contact with the alloy, completely different from the classical structure of the ioz which corresponds to the presence of a uniform volume fraction of the precipitated oxide within the alloy in the absence of a layer of oxide intermediate between the ioz and the alloy. Moreover, the depth of the ioz was not uniform, especially after 24 h oxidation and had no relationship with the orientation of the grains (Fig. 2f). This is not considered a result of changes in the alloy composition in a lateral direction (the alloys were annealed for long times to avoid this possibility), but of the presence of the SiO2 layer at the base of the ioz, which may have formed at different reaction stages over different locations over the surface.

To obtain a three-dimensional structure of the SiO_2 particles, the oxidized samples

were examined also after a deep etching by the $CuSO_4$ solution (Figs. 4-6). The particles of SiO_2 in the anomalous ioz close to the gas side were spherical (Fig. 4a), while underneath they were vermicular (Fig. 4b) as verified by etching the sample partly (Fig. 4c). Actually, these vermicular particles formed net structures parallel to the alloy surface. Within the anomalous ioz, both types of particles were wrapped up by the alloy matrix. By etching the whole sample to a certain depth, the net-like structure of SiO_2 was more evident (Fig. 5a), while some SiO_2 pieces presented many fissures (Fig. 5b). When the ioz was completely removed, a continuous layer of SiO_2 became visible. The morphology of the two sides (Figs. 6a-6b) of the layer showed again that this SiO_2 layer was irregular.

Cross-sections of Fe-9Si oxidized for different times are shown in Fig. 7. After 10 h oxidation, moving from the surface to the substrate there was an anomalous ioz followed by a continuous SiO_2 layer. After 24 h oxidation the depth of the SiO_2 layer increased quite significantly (Fig. 7b), while at some places the SiO_2 layer was protruding into the alloy (Fig. 7c): this tends to improve the alloy/scale adhesion by increasing the actual contact area between the scale and the base alloy [25]. These spots were both intergranular and intragranular, indicating that the oxidation along the grain boundaries was not faster than that of the interior of the grains. Therefore, the effect of the gain boundaries on the oxidation of Fe-Si alloys does not appear to be significant in the present case, contrary to the oxidation of Co-Al-W-B superalloys [26].

The morphologies of the scales formed on Fe-13Si after different oxidation times are shown in Fig. 8. In all cases this alloy formed a continuous layer of SiO_2. The layer formed after 4 h was divided into two sub-layers, with an outer zone darker and more compact than the inner zone and particles of metallic iron distributed throughout the whole SiO_2 layer (Fig. 8a). Conversely, after 24 h oxidation the whole SiO_2 layer was covered by a continuous layer of pure iron (Fig. 8c) which, however, together with parts of the SiO_2 layer, tended to crack and also to spall off from the silica layer probably during cooling (Figs. 8b-d).

4. Discussion

The conditions for the stability of the various possible forms of oxidation of the present alloys are examined below with reference to the classical conditions for the transitions

among them.

4.1 Transition from internal to external oxidation

According to the phase diagram shown in Fig. 9, which was calculated with the help of the thermodynamic data [27,28], the oxygen pressure supplied by the present binary H_2-CO_2 mixture was of 10^{-20} atm: this value, marked by a dot in Fig. 9, is lower than the dissociation pressure of the iron oxides, but above that of silicon oxide. Thus, the only oxide that can form during this experiment is SiO_2. At this temperature silica is generally amorphous [29], in good agreement with the XRD spectrum (Fig. 3) which shows only the spectral lines of the base alloy.

The oxidation of binary single-phase A-B alloys dilute in B, in which A behaves as a noble element and B is the reactive component forming an oxide BO_ν, generally produces an internal oxidation of B within an A matrix following the parabolic rate law [30,31]. As the concentration of B increases, the internal oxide particles dispersed in the ioz tend to develop a continuous external BO_ν layer: the critical concentration of B (mole fraction) required for the transition from the internal to the external oxidation of B is denoted as $N_B°^*$ [23,30,31].

The first basic equation needed for the calculation of $N_B°^*$ is related to the kinetics of internal oxidation. In the absence of external scales of the oxide of A, this equation has the form

$$\frac{N_O^s}{\nu N_B^o} = \frac{G(\gamma)}{F(\gamma)} \qquad (1)$$

where N_O^s is the concentration of oxygen (mole fraction) dissolved in A at the alloy/gas interface and γ a kinetic parameter related to the parabolic constant for the advancement of the front of internal oxidation, k_ξ, expressed as

$$\xi^2 = k_\xi t = 4\gamma^2 D_O t \qquad (2)$$

where ξ is the thickness of the ioz, D_O is the diffusion coefficient of oxygen in A and t is time. Moreover, $h = \gamma\varphi^{1/2}$, where $\varphi = D_O/D_B$ and where D_B is the diffusion coefficient of B in A. Finally, $G(\gamma)$ and $F(\gamma)$ are two auxiliary functions defined as [32]

$$G(\gamma) = \pi^{1/2}\gamma \exp(\gamma^2)\,\mathrm{erf}(\gamma) \quad (3)$$

and

$$F(\gamma) = \pi^{1/2}\gamma \exp(\gamma^2)\,\mathrm{erfc}(\gamma) \quad (4)$$

The second basic equation, proposed by Wagner in connection with a criterion for the transition from the internal to the external oxidation of B, is based on a critical value of the volume fraction of internal oxide, f_v^*, above which the internal oxidation of B is prevented and has the form

$$N_B^{o*} = f_v^* \frac{F(h)}{\rho} \quad (5)$$

where ρ is the ratio between the molar volume of BO_v and that of the alloy. After a work by Rapp [33] on the oxidation of Ag-In alloys, f_v^* is generally set equal to 0.3.

The data needed for the calculation of N_B^{o*} include the diffusion coefficient of oxygen and silicon in the alloy, D_O [32] and D_{Si} [35] (cm^2/s), given by

$$D_O = 1.79\times10^{-3} \exp\left(\frac{-85700}{RT}\right) \quad (6)$$

and

$$D_{Si} = 0.735\times(1+12.4\times N_{Si}) \exp\left(\frac{-219880}{RT}\right) \quad (7)$$

where N_{Si} is the mole fraction of silicon in the alloy.

The mole fraction of oxygen dissolved in α-Fe under the oxygen pressure for the Fe-FeO equilibrium, $P(O_2)^{eq}$, denoted as N_O^{so}, is given by [36]

$$N_O^{so} = 1.5\times\exp\left(\frac{-128330}{RT}\right) \quad (8)$$

At 800°C, $P(O_2)^{eq}$ is equal to 2.03×10^{-20} atm and N_O^{so} to 8.48×10^{-7}. The solubility of oxygen in α-Fe under the present gas phase oxygen pressure, $P(O_2)^{g}$, denoted as N_O^{s}, is calculated according to Sievert's law [37] in the form

$$N_O^{s} = N_O^{so}\left[\frac{P(O_2)^{g}}{P(O_2)^{eq}}\right]^{1/2} \quad (9)$$

and at 800°C becomes equal to 5.96×10^{-7}. The final parameter needed is the ratio between the molar volumes of iron and silica, which, using the density typical of silica glass (2.2 gcm^{-3}) yields ρ = 3.846. Introduction of the previous parameters into Eqs.(1) and (5) with ν = 2 yields finally $N_B°^* = 1.5 \times 10^{-2}$. Although this value may be somewhat inaccurate due to the uncertainty in the numerical values of the various parameters involved, such as in particular the molar volume of amorphous silica, it may be considered as sufficiently correct for the comparison with the experimental results in view of the large difference between the two data and of the peculiar nature of the internal oxidation observed for these alloys.

The silicon contents of the three Fe-Si alloys used in the present study are significantly larger than $N_B°^*$ value calculated above, so that in principle they are all expected to form continuous external SiO_2 scales. This prediction is not in agreement with the present experimental results because a continuous layer of silica over the alloy surface at the beginning of the experiment has only been observed on Fe-13Si, while both Fe-5Si and Fe-9Si underwent an internal oxidation of silicon, even if this was associated with the formation of a continuous silica layer at the interface between the ioz and the underlying alloy, clearly grown only after an initial stage of internal oxidation (for times up to 4 h for Fe-5Si, when the silica layer was clearly discontinuous, Fig. 2a). The calculated critical content of silicon needed for the formation of the external SiO_2 scale is at least 5 times smaller than that of the experimental result (compared with Fe-9Si). Therefore, the actual oxidation behavior of the two more dilute alloys is more complex than expected, while the critical silicon content calculated above for binary Fe-Si alloys is significantly smaller than the experimental value, in agreement with the result of the oxidation of Fe-Si alloys at 850 ^oC under a controlled oxygen pressure obtained by Onishi et al. [21].

The large discrepancy between the calculated and experimental values of $N_B°^*$ may have different reasons. The possibility that this is due to the fact that the species diffusing in the alloy may be water rather than oxygen is ruled out on the basis that water molecule is larger than O atoms and that the solubility of water in the alloy should be completely negligible. Also the fact that the fluxes of oxygen and Si at the internal oxidation front are largely different in view of the much larger value of D_O as compared to D_{Si} is considered irrelevant. In fact, this implies only that Si remains essentially immobile in front of the fast

penetration of oxygen, but does not affect the balance between the fluxes at the internal oxidation front. A first possible real explanation is related with the thickness of the anomalous ioz observed for Fe-5Si after 4 h oxidation, around 3 μm (see Fig. 2a), which corresponds to a parabolic rate constant of internal oxidation, k_ξ, equal to 6.25×10^{-12} $cm^2 s^{-1}$. However, a calculation of γ using Eq. 1 setting $N_{Si}° = 0.05$ and using the data reported above yields $k_\xi = 5.31 \times 10^{-14}$ $cm^2 s^{-1}$, so that the thickness of the ioz after 4 h should be equal to 0.28 μm, i.e. much less than the experimental value. This result is especially surprising as the sample oxidized for 4 h shows already a trace of silica layer beneath the ioz, which in principle should already reduce the rate of advancement of the internal oxidation front with respect to the case of a complete absence of this layer. Thus, Fe-5Si alloy undergoes an internal oxidation significantly faster than expected on the basis of the relevant parameters involved, while the formation of a silica layer is clearly hindered and occurs only after some time and beneath a zone of anomalous internal oxidation. A similar situation applies also to the oxidation of Fe-9Si because the thickness of the ioz measured after 10 h oxidation is of about 4 μm, which corresponds to $k_\xi = 4.4 \times 10^{-12}$ $cm^2 s^{-1}$. Again, the calculation of γ with Eq.(1) with $N_{Si}° = 0.09$ yields $k_\xi = 1.67 \times 10^{-14}$ $cm^2 s^{-1}$, so that the thickness of the ioz after 10 h should be of only 0.24 μm, still much less than the experimental value.

A possible explanation of these observations is related to the large volume increase associated with the precipitation of SiO_2: the important stress produced in this way may produce a significant increase of the diffusion coefficient of oxygen through the ioz, possibly along physical discontinuities produced inside the alloy matrix, which would correspond to a faster rate of displacement of the front of internal oxidation. The faster diffusion of oxygen through the ioz may also be assisted by the formation of silica particles of complex shape and at least partly interconnected, as reported for a number of cases by Stott and Wood [38]. In fact, according to their model, the interface between precipitates and the matrix metal may provide an alternative diffusion path for the penetration of oxygen, much faster than the normal diffusion through the bulk of the alloy.

Another possibly important reason for the observed large discrepancy between the calculated and experimental values of $N_B°*$ is connected with the very low rate of growth of SiO_2 scales, which may favor the formation of isolated particles and also prevent their

coalescence to form a continuous layer, especially during the initial stage, when the oxidation rate is fastest. As a consequence, the formation of a continuous layer of this oxide on the surface of Fe-Si alloys requires in practice silicon contents significantly larger than the critical value predicted theoretically.

In fact, the oxidation of Fe-Si alloys with silicon contents above the critical value needed for the transition from the internal to external oxidation as calculated above, but still insufficient to sustain the growth of the SiO_2 layer, produces an anomalous ioz associated with the presence of a continuous silica layer at the interface between the anomalous ioz and the alloy during an initial stage, but broken down afterwards, as observed for Fe-5Si and Fe-9Si. This phenomenon, not reported so far in the oxidation of Si-containing alloys, needs a further investigation and may also be related with the amorphous phase structure of SiO_2.

4.2 The formation mechanisms of the anomalous internal oxidation zone

When the concentration of silicon in an Fe-Si alloy is low, the precipitates of SiO_2 in the internal oxidation zone are all spherical [21], as observed for Cu-Si alloys with silicon contents less than 0.62 at.% [39]. However, the morphology of SiO_2 in the anomalous internal oxidation zone in the present work is more complex, especially for Fe-5Si. In fact, besides the spherical particles, the alloy shows also the formation of a branched SiO_2 network. A similar phenomenon has also been observed in the oxidation of Fe-5.83 at.% Si [18, 19] under oxygen pressures sufficiently large to form the iron oxides. These SiO_2 particles with complex shapes resulted from a breakdown of the SiO_2 layer connected directly with the base alloy. Fig. 10 shows a schematic representation of the breakdown mechanism of the SiO_2 layer at the anomalous internal oxidation front during oxidation.

During the initial oxidation stage (Fig. 10a), SiO_2 nucleates and grows quickly within the alloy surface layer forming particles with spherical shape following the parabolic rate law, similar to the early stage of oxidation of Fe-1Si under a low oxygen pressure [38]. This indicates that the inward diffusion of oxygen is the rate-controlling step, in agreement with the proposal of Wagner [31] about the internal oxidation of dilute alloys. During this period, due to the large oxygen potential within the ioz, the flux of oxygen into the alloy is larger than that of silicon diffusing to the ioz front from the bulk alloy, causing the in-situ oxidation

of silicon. After 4 h oxidation (Fig. 10b), an almost continuous layer of SiO_2 forms at the front of the internal oxidation zone and the oxidation rate slows down significantly. This implies that with the increase of the depth of the ioz, the gradient of oxygen potential decreases leading to the decrease of the oxygen flux at the alloy/ioz interface, so that the flux of silicon becomes relatively higher than that of oxygen, leading to the formation of a protective SiO_2 layer at the interface between the ioz and the alloy.

However, the continuous SiO_2 layer formed is not pure, but contains some iron in solution, possibly behaving like Cu dissolved in silica [41]. Later on, during the sintering period, silica tends to contract and expel the iron atoms. At the same time, it cracks and ruptures into pieces due to the shrinkage stresses and then grows into net-shaped and spherical particles when the supply of silicon from the base alloy is not sufficient to maintain the protective layer (Figs. 10c-d). When the supply of silicon is sufficient, the layer of SiO_2 remains stable but becomes thinner. At the same time, oxygen diffuses through the broken SiO_2 areas moving the anomalous internal oxidation front forward until the SiO_2 layer is healed. The breaking and healing processes are repeated until the outward diffusion of silicon is sufficient to sustain fully the growth of SiO_2 (Fig. 10e). In the kinetic curve this period is reflected by an irregular behavior. The irregular kinetics have also been discussed by Tomlinson and Yates [42]. Contrary to the case of oxidation of the alloys Cu-4 at.%Si [43] and Fe-5.82 at.% Si [14], in which the interconnected fractal branches of SiO_2 extended into the bulk alloy, the network of SiO_2 grown on Fe-5Si observed in this work is parallel to the alloy surface.

The formation of nodules of the solvent metal on the surface of binary alloys undergoing an internal oxidation of the most reactive component when the base metal has a noble behavior has been reported frequently [44-46]. However, in the present case iron forms a continuous layer outside the SiO_2 scale. There are many proposals for nodules formation, including the Nabarro-Herring creep mechanism [44], as well as the increased dislocation density for the deformation due to the internal oxidation [45]. However, the formation of the external iron layer is due to the permeability of iron through the amorphous SiO_2 layer [1]. The sources of iron are proposed to be two: one is from the impure SiO_2 layer containing some iron. During the following sintering period, the SiO_2 layer contracts and

expels iron which later nucleates and grows to spherical particles and moves out. The other source is the base alloy: in this case the driving force for diffusion is the activity difference [1] and the compressive tension generated during oxidation [45]. Adachi et al. [1] proposed that iron is transported through the SiO_2 layer in the form of atoms rather than of ions.

4.3 Spallation of the scale

The main disadvantage of some protective scales is their tendency to peel off from the base alloy, especially during cooling. A severe spallation of Al_2O_3 and Cr_2O_3 layers from the base alloys free from reactive elements has often been reported [47,48]. The SiO_2 layer formed on Fe-13Si in this research spalled off severely even after only 4 h oxidation. The poor scale adhesion is associated with the high growth stresses accumulated during oxidation as well as with the large differences in the thermal expansion coefficients between the alloy and SiO_2 (equal to $1.2x10^{-5}$ /^oC for α-Fe in the temperature range of 0~100 ^oC, and to $5.8x10^{-7}$ /^oC for amorphous SiO_2 at 16~1000 ^oC [49]). It has been reported that spalling and cracking of the SiO_2 layer at the oxide/alloy surface is more dangerous than if it occurs within the oxide itself [50]. The vacancies injected into the metal at the alloy/scale interface by the outward growth of the SiO_2 scale tend to precipitate as voids which are considered detrimental for mechanical scale adhesion. However, this is not the case here, since the failure occurs cohesively within the SiO_2 layer, and it is more evident in the scale after 4 h oxidation. It has been postulated [51] that the fracture strength of SiO_2/alloy interface is higher than that within the SiO_2 itself.

5. Conclusions

The oxidation of three Fe-Si alloys at 800 ^oC in a gas mixture providing an oxygen pressure of 10^{-20} atm, which is below the dissociation oxygen pressure of iron oxides, produced an anomalous internal and external oxidation of silicon. The oxidation kinetics for the three Fe-Si alloys are generally rather irregular, with the instantaneous parabolic rate parameter changing with time, but the oxidation rate decreases when the silicon level increased. The silicon content of Fe-5Si is not sufficient to sustain the formation of a continuous and stable SiO_2 layer at the internal oxidation front, which broke down partly and later re-healed: repetition of these two processes is responsible for the irregular kinetics

observed. The internal oxidation precipitates grown on Fe-5Si within the anomalous ioz are partly spherical and partly interconnected forming fractal dendritic structures. The SiO_2 layers grown on Fe-9Si and Fe-13Si are stable, providing a good oxidation resistance. The critical content of silicon needed for the formation of the external SiO_2 layer is much higher than the calculated results according to an extension of Wagner's theory. However, the SiO_2 layer formed on Fe-13Si tends to spall off during cooling. In addition, a layer of pure iron forms on the SiO_2 layer by oxidation of Fe-13Si as a result of an outward migration of iron.

Acknowledgments: Financial supports by NSFC of China under the research projects (Nos. 50971129 and 51371183) are gratefully acknowledged.

REFERENCES

1. T. Adachi, G.H. Meier, Oxidation of iron-silicon alloys, Oxid. Met. 27 (1987) 347-366.
2. T. Nishimoto, K. Honda, Y. Kondo, K. Uemura, Effects of Si content on the oxidation behavior of Fe-Si alloys in air, Mater. Sci. Forum 696 (2011) 126-131.
3. M. Fukumoto, S. Hayashi, S. Maeda, T. Narita, The effect of Si concentration and temperature on initial stage of high temperature oxidation of Fe-low Si alloys, Tetsu to Hagane 85 (1999) 878-884.
4. M. Fukumoto, S. Maeda, S. Hayashi, T. Narita, The effect of temperature and water vapor on the initial stage of high temperature oxidation of an Fe-1.5mass%Si alloy, Tetsu to Hagane 86 (2000) 526-533.
5. K. Kusabiraki, R. Watanabe, T. Ikehata, M. Takeda, T. Tonishi, X.P. Guo, High-temperature oxidation behavior and scale morphology of Si-containing steels, ISIJ Int. 47 (2007) 1329-1334.
6. A. Lashin, O. Schneeweiss, Y. Houbaert, Effect of ambient air pressure on the oxidation kinetics of Fe-6 at.% Si alloy, Corros. Sci. 50 (2008) 2580-2587.
7. L.L. Liu, Q.Q. Guo, Y. Niu. Transition between different oxidation modes of binary Fe-Si aloys at 600-800 ^{o}C in Pure O_2, Oxid. Met. 79 (2013) 201-224.
8. A.R. Lashin, O. Schneeweiss, Surface oxidation of Fe-Si alloy, Czech. J. Phys. A. 56 (2006) E23-29.
9. J. Porcayo-Calderon, E. Brito-Figueroa, J.G. González-Rodŕiguez, Oxidation behaviour of Fe-Si thermal spray coatings, Mater. Lett. 38 (1999) 45-53.
10. A. Atkinson, A theoretical analysis of the oxidation of Fe-Si alloys, Corros. Sci. 22 (1982) 87-102.
11. P.T. Moseley, G. Tappin, J.A.A. Crossley, J.C. Riviere, The microstructure of the scale forming on dilute iron-silicon alloys in carbon-dioxide, Corros. Sci. 23 (1983) 901-920.
12. P.T. Moseley, G. Tappin, J.C. Riviere, The oxidation of dilute iron-silicon alloys(Si<1 wt.%) in carbon dioxide, Corros. Sci. 2 (1982) 69-86.

13. M. Fukumoto, S. Maeda, S. Hayashi, T. Narita, Effect of water vapor on the oxidation behavior of Fe-1.5Si in air at 1073 and 1273 K, Oxid. Met. 55 (2001) 401-422.
14. M.A.A. Motin, J. Zhang, P.R. Munroe, D.J. Young, Internal oxidation and metal dusting of Fe-Si alloys, Corros. Sci. 52 (2010) 3280-3286.
15. M.A.A. Motin, J. Zhang, D.J. Young, Simultaneous corrosion of Fe-Si Alloys by carbon and oxygen, J. Electrochem. Soc. 157 (2010) C375-C381.
16. T. Ban, K. Bohnenkamp, H.J. Engell, The formation of protective films on iron-silicon alloys, Corros. Sci. 19 (1979) 283-293.
17. K. Yanagihara, S. Suzuki, S. Yamazaki, Microscopic features in the transition from external to internal oxidation in an Fe-6 mol.% Si alloy annealed under various H_2O-H_2 atmospheres, Oxid. Met. 57 (2002) 281-296.
18. H. Li, J.Q. Zhang, D.J. Young, Oxidation of Fe-Si, Fe-Al and Fe-Si-Al alloys in CO_2-H_2O gas at 800 ^{o}C, Corros. Sci. 54 (2012) 127-138.
19. H. Li, J.Q. Zhang, D.J. Young, Oxidation of Fe-Si alloys in CO_2-H_2O atmospheres, Mater. High Temp. 28 (2011) 297-301.
20. K. Yanagihara, S. Yamazaki, Characterization of oxidation behavior at Fe-Si alloy surface, Nippon steel technical report 100 (2011) 27-32.
21. T. Onishi, S. Nakakubo, M. Takeda, Calculation of internal oxidation rate equations and boundary conditions between internal and external oxidation in Si containing steels, Mater. Trans. 51 (2010) 482-487.
22. T.B. Massalski, J.L. Murry, L.H. Bennett, H. Baker, Binary Alloys Phase Diagrams, ASM, Materials Park, Ohio, 1986.
23. C. Wagner, Reaktionstypen bei der oxydation von Legierungen, Z. Elektrochem. 63 (1959) 772-782.
24. D. Young, High Temperature Oxidation and Corrosion of Metals, first ed., Elsevier corrosion series, Cambridge, 2008.
25. W. Wang, B. Zhang, C. Zhou, Formation and oxidation resistance of Hf and Al modified silicide coating on Nb-Si based alloy, Corros. Sci. 86 (2014) 304-309.
26. L. Klein, B. von Bartenwerffer, M.S. Killian, P. Schmuki, S. Virtanen, The effect of grain boundaries on high temperature oxidation of new γ'-strengthened Co-Al-W-B superalloys, Corros. Sci. 79 (2014) 29-33.
27. I. Barin, Thermochemical Data of Pure Substances, first ed. VCH Verlags Gesellschaft, Weinheim, 1989.
28. Landolt-Börnstein, Thermodynamic Properties of Inorganic Material, first ed., Springer-Verlag Berlin-Heidelberg, Berlin, 1999.
29. A.G. Revesz, B.J. Mrstik, H.L. Hughes, D. McCarthy, Structure of SiO_2 films on silicon as revealed by oxygen transport, J. Electrochem. Soc. 133 (1986) 586-592.
30. C. Wagner, Übcrlegungen zum Übergang vom linearen zum parabolischen Zeitgesetz der Oxydation eines Metalls zu einem Oxid mit Metalldefizit, Ber. Bunsen-Ges. 8 (1966) 775-780.
31. R.A. Rapp, Kinetics, microstructure and mechanism of internal oxidation-its effect and prevention in high temperature alloy oxidation, Corros. 21 (1965) 382-401.
32. J. Crank, The Mathematics of Diffusion, first ed., Clarendon Press, Oxford, 1965.
33. R.A. Rapp, The transition from internal to external oxidation and the formation of interruption bands in silver-indium alloys, Acta Metall. 9 (1961) 730-741.

34. J. Takada, S. Yamamoto, S. Kikuchi, M. Adachi, Internal oxidation of Fe-Al alloys in the α-phase region, Oxid. Met. 25 (1986) 93-105.
35. W.F. Gale, T.C. Totemeier, Diffusion in Smithells Metals Reference Book, eighth ed., Butterworth-Heinemann, Elsevier, 2004.
36. W. Frank, H.J. Engell, A. Seeger, Solublity and intersititial migration of oxygen in bcc iron, Trans. Met. Soc. AIME 242 (1968) 749-750.
37. D.R. Gaskell, Introduction to the Thermodynamics of Materials, fifth ed., Taylor & Francis, 2008.
38. F.H. Stott, G.C. Wood, Internal oxidation, Mater. Sci. Technol. 4 (1988) 1072-1078.
39. P. Bolsaiti, M. Kahlweit, Internal oxidation of Cu-Si alloys, Acta Metall. 15 (1967) 765-772.
40. M. Auinger, A. Vogel, D. Vogel, M. Rohwerder, Early stages of oxidation observed by in situ thermogravimetry in low pressure atmospheres, Corros. Sci. 86 (2014) 183-188.
41. J. Kapteijn, S.A. Couperus, J.L. Meijerin, High-temperature oxidation of copper with up to 4.1wt.% Si, Acta Metall. 17 (1969) 1311-1315.
42. W.J. Tomlinson, J. Yates, High-temperature oxidation kinetics of Cu-Si alloys containing up to 4.75 wt.% Si in p_{O_2}=0.01 atm and pure CO_2, Oxid. Met. 12 (1978) 323-329.
43. M. Backhaus-Ricoult, L. Samet, M. Thomas, M.F. Trichet, D. Imhoff, Changes in Cu-silica interfacial chemistry with oxygen chemical potential, Acta Mater. 50 (2002) 4191-4204.
44. S. Guruswamy, S.M. Park, J.P. Hirth, R.A. Rapp, Internal oxidation of Ag-In alloys-stress relief and the infulence of imposed strain, Oxid. Met. 26 (1986) 77-100.
45. D.L. Douglass, A critique of internal oxidation in alloys during the post-wagner era, Oxid. Met. 44 (1995) 81-111.
46. D.L. Douglass, B.Z. Zhu, F. Gesmundo, Internal-oxide-band formation during oxidation of Ag-Mg alloys, Oxid. Met. 38 (1992) 356-384.
47. F.A. Golightly, F.H. Stott, G.C. Wood, The influence of yttrium additions on the oxide-scale adhesion to an iron-chromium-aluminum alloy, Oxid. Met. 10 (1976) 163-187.
48. Y. Zhang, D.A. Shores, Study of cracking and spalling of Cr_2O_3 scale formed on Ni-30Cr alloy, Oxid. Met. 40 (1993) 529-553.
49. J.G. Speight, Lange's Handbook of Chemistry, sixteenth ed., McGraw-Hill Professional, New York, 2005.
50. H.E. Evans, R.C. Lobb, Conditions for the initiation of oxide-scale cracking and spallation, Corro. Sci. 24 (1984) 209-222.
51. F.H. Stott, G.J. Gabriel, F.I. Wei, G.C. Wood, The development of silicon-containing oxides during the oxidation of iron-chromium-base alloys, Mater. Corros. 38 (1987) 521-531.

Figure and Table Captions

Fig. 1 Parabolic plots of the kinetic curves for the Fe-xSi (x=5, 9, 13 at.%) oxidized in the H_2-CO_2 mixture at 800°C for 24 h.
(a): General plots; (b): Enlarged plots for Fe-9Si and Fe-13Si.

Fig. 2 Cross sections of Fe-5Si oxidized in the H_2-CO_2 mixture at 800°C for the times up to 24 h.
(a): 1.5 h (BEI); (b): 4 h (BEI); (c): 18 h (BEI); (d): 24 h (BEI); (e): Enlarged view of (d) (BEI); (f): 24 h, etched by $CuSO_4$ (SEM).

Fig. 3 XRD spectrum of the scale of Fe-5Si oxidized in the H_2-CO_2 mixture at 800°C for 24 h.

Fig. 4 Surface morphologies of Fe-5Si oxidized in the H_2-CO_2 mixture at 800°C for 24 h.
(a): Original surface after oxidized (BEI); (b): Surface after polished down the anomalous ioz to some depth (BEI); (c): Etched the anomalous ioz partly by $CuSO_4$ (SEM).

Fig. 5 Deep-etched surface morphologies (SEM) of Fe-5Si oxidized in the H_2-CO_2 mixture at 800°C for 24 h by $CuSO_4$.
(a): General view ; (b): Enlarged view of the SiO_2 particles in the anomalous ioz.

Fig. 6 Deep-etched surface morphologies (SEM) of Fe-5Si oxidized in the H_2-CO_2 mixture at 800°C for 24 h by $CuSO_4$. (a): General view of SiO_2 scale; (b): The reverse side of SiO_2 scale.

Fig. 7 Cross sections (BEI and OM) of Fe-9Si oxidized in the H_2-CO_2 mixture at 800°C for the times up to 24 h.
(a): 10 h (BEI); (b): 24 h (BEI); (c): 24 h, etched by $CuSO_4$ (OM).

Fig. 8 Cross sections (BEI) and surface morphology (SEM) of Fe-13Si oxidized in the H_2-CO_2 mixture at 800°C.
(a): Cross section for 4 h; (b): Surface morphology for 24 h; (c): Cross section for 24 h; (d): Enlarged view of (c).

Fig. 9 Superimposed phase diagrams of the binary Fe-O and Si-O systems [27,28] with an indication of the oxygen pressure used in the present work by a dot.

Fig. 10 Schematics of the development of the anomalous ioz and the breakdown of the SiO_2 layer on Fe-5Si.
(a): Initial stage before the formation of the SiO_2 layer; (b): Formation of the SiO_2 layer; (c): Appearance of fissures in the SiO_2 layer viewed parallel to the layer; (d): Formation of the net-shaped and spherical particles viewed parallel to the layer; (e): Reformation of the SiO_2 layer.

Table 1 Nominal and actual compositions of three Fe-xSi alloys measured by ICP spectrometry analysis

Nominal	Actual (at.% / wt.%)
Fe-5Si	Fe-5.35 / 2.75Si
Fe-9Si	Fe-9.47 / 4.97Si
Fe-13Si	Fe-13.00 / 6.96Si

Highlights

► The Fe-(5-13at.%) Si alloys oxidized at 10^{-20} atm O_2 at 800 °C form a SiO_2-rich layer.

► The critical Si content to form a SiO_2 layer was 1.5 at.% (calculated result).

► Fe-5Si formed an anomalous internal oxidation zone with net-shaped SiO_2 structure.

► The SiO_2 scale grown on Fe-9/13Si alloys was stable but spalled off during cooling.

Figure

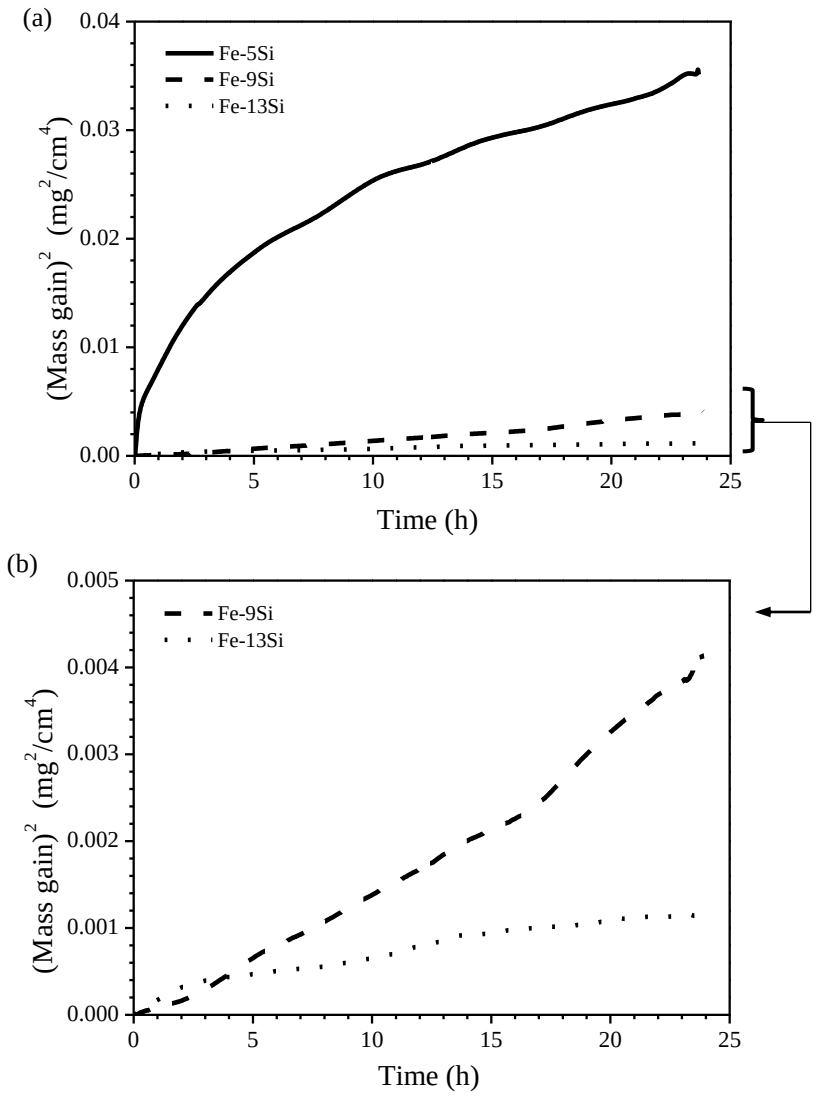

Fig. 1 Parabolic plots of the kinetic curves for the Fe-xSi alloys (x=5, 9, 13 at.%) oxidized in the H_2-CO_2 mixture at 800°C for 24 h.
(a): General plots; (b): Enlarged plots for Fe-9Si and Fe-13Si.

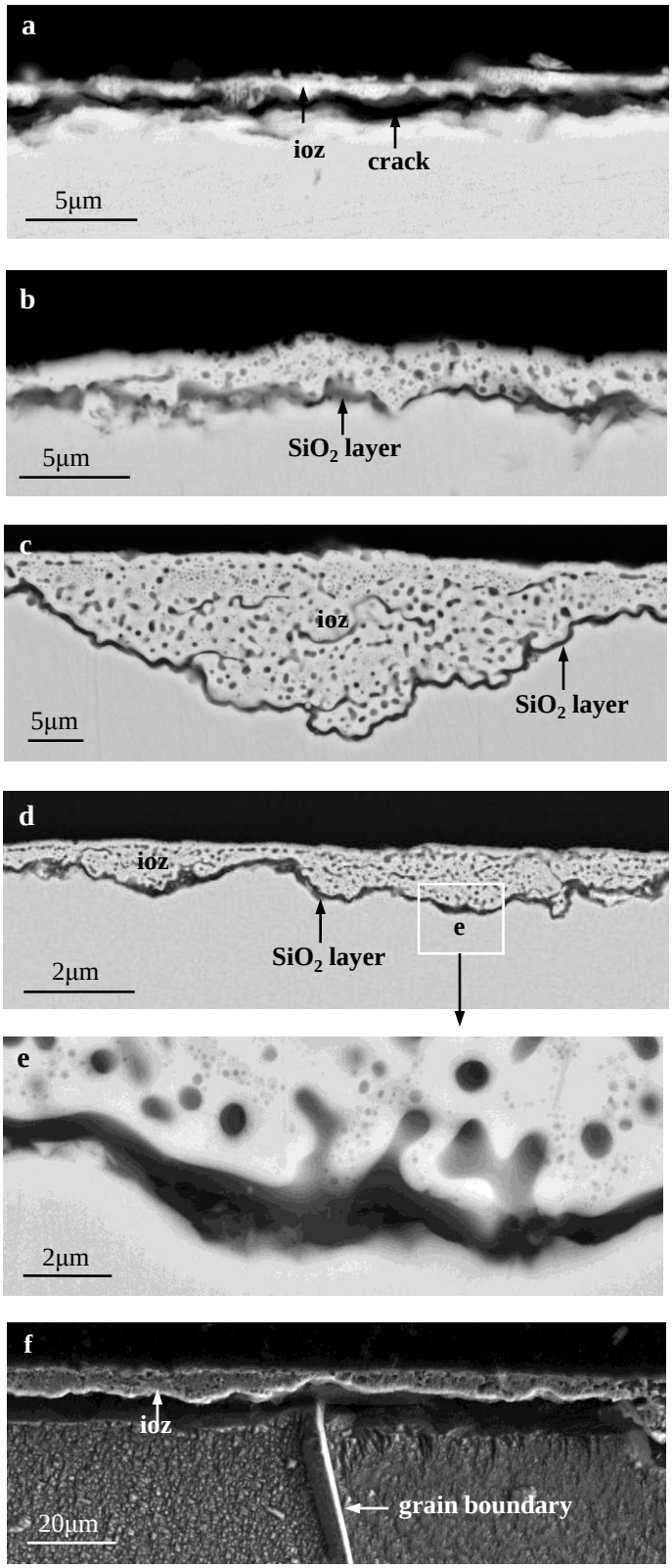

Fig. 2 Cross sections of Fe-5Si oxidized in the H_2-CO_2 mixture at 800 ^oC for the times up to 24 h. (a): 1.5 h (BEI); (b): 4 h (BEI); (c): 18 h (BEI); (d): 24 h (BEI); (e): Enlarged view of (d) (BEI); (f): 24 h, etched by $CuSO_4$ (SEM).

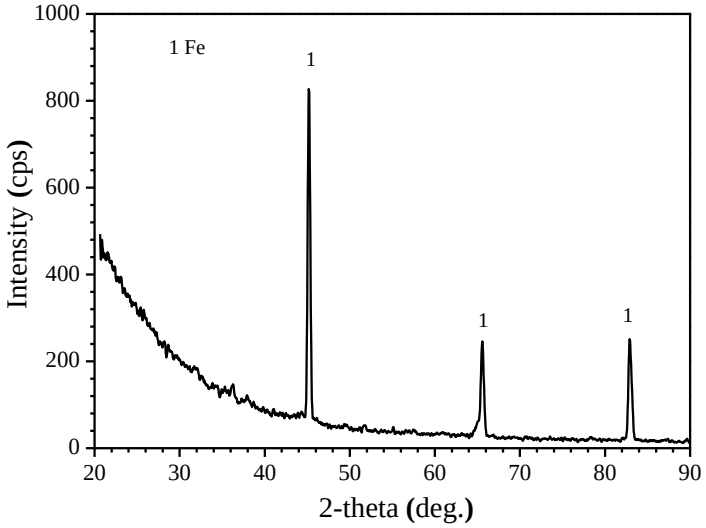

Fig. 3 XRD spectrum of the scale of Fe-5Si oxidized in the H_2-CO_2 mixture at 800 ^oC for 24 h.

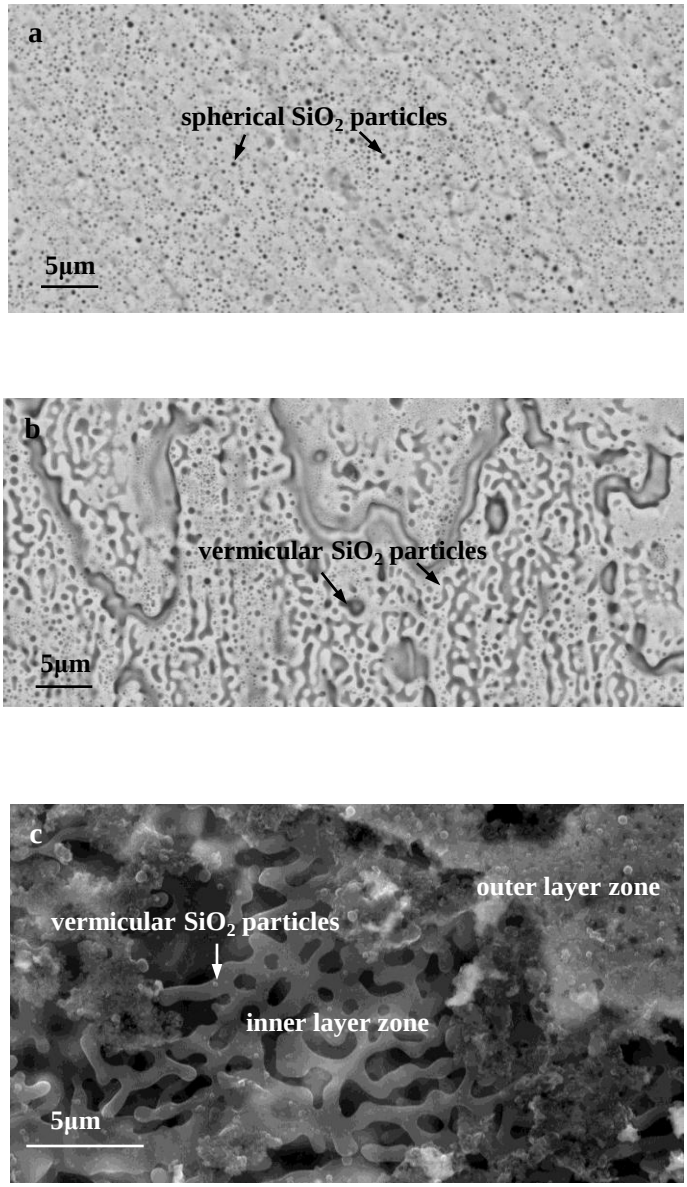

Fig. 4 Surface morphologies of Fe-5Si oxidized in the H_2-CO_2 mixture at 800 °C for 24 h.

(a): Original surface after oxidized (BEI); (b): Surface after polished down the anomalous ioz to some depth (BEI); (c): Etched the anomalous ioz partly by $CuSO_4$ (SEM).

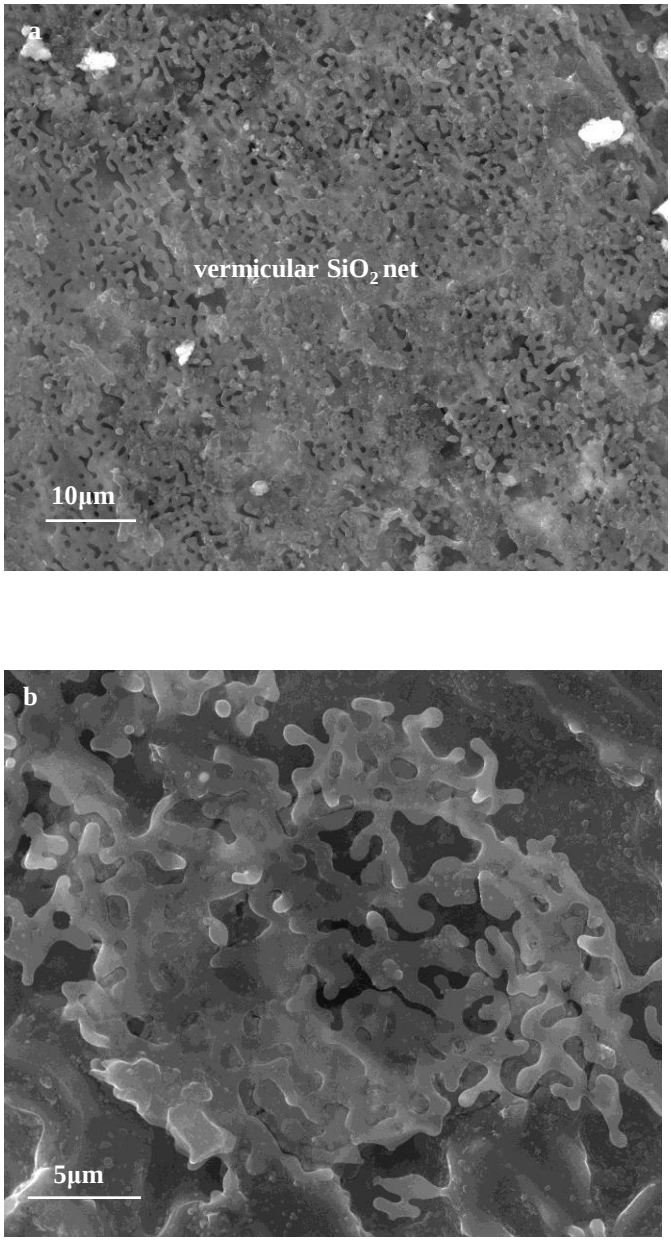

Fig. 5 Deep-etched surface morphologies (SEM) of Fe-5Si oxidized in the H_2-CO_2 mixture at 800 ^oC for 24 h by $CuSO_4$.

(a): General view; (b): Enlarged view of SiO_2 in the anomalous ioz.

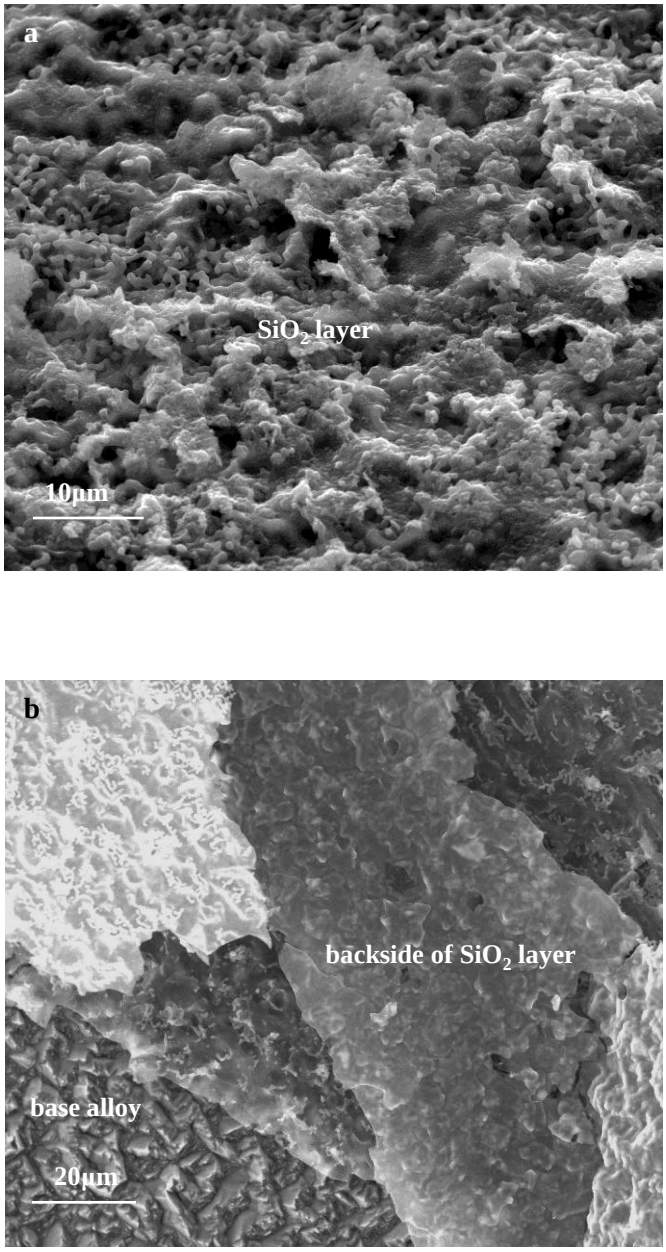

Fig. 6 Deep-etched surface morphologies (SEM) of Fe-5Si oxidized in the H_2-CO_2 mixture at 800 ^oC for 24 h by $CuSO_4$.
(a): General view of SiO_2 scale; (b): The reverse side of SiO_2 scale.

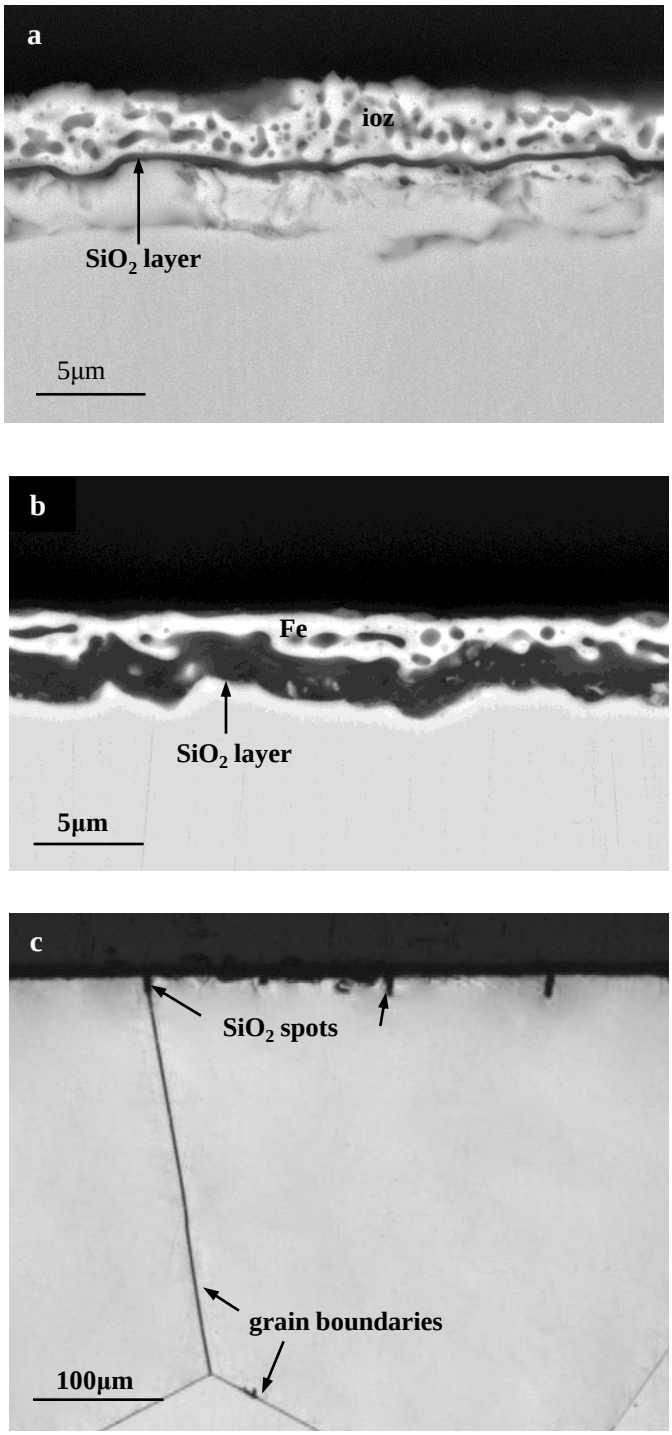

Fig. 7 Cross sections (BEI and OM) of Fe-9Si oxidized in the H_2-CO_2 mixture at 800 ^oC for the times up to 24 h.

(a): 10 h (BEI); (b): 24 h (BEI); (c): 24 h, etched by $CuSO_4$ (OM).

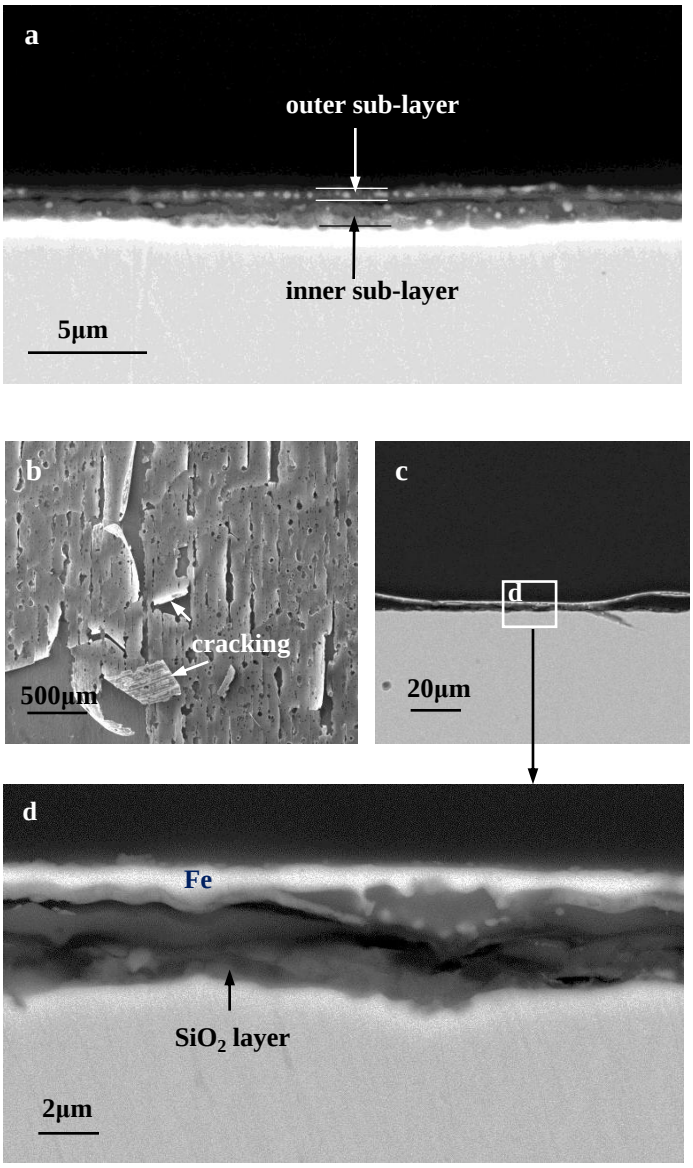

Fig. 8 Cross sections (BEI) and surface morphology (SEM) of Fe-13Si oxidized in the H_2-CO_2 mixture at 800 ^{o}C.

(a): Cross section for 4 h; (b): Surface morphology for 24 h; (c): Cross section for 24 h; (d): Enlarged view of (c).

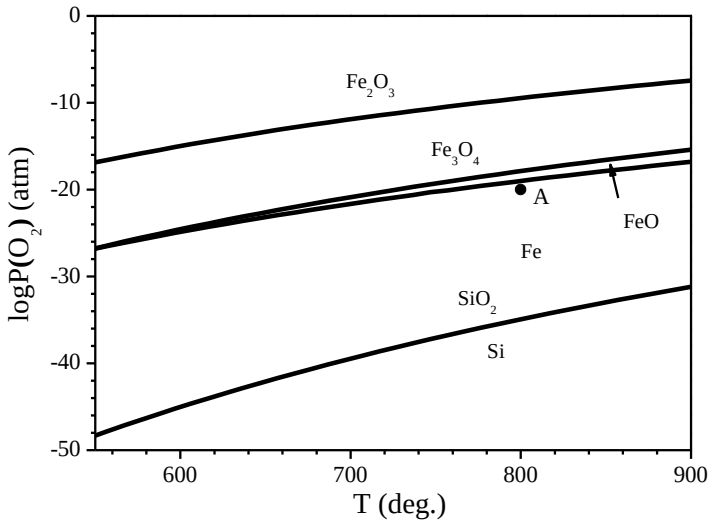

Fig. 9 Superimposed phase diagrams of the binary Fe-O and Si-O systems [27,28] with an indication of the oxygen pressure used in the present work by a dot.

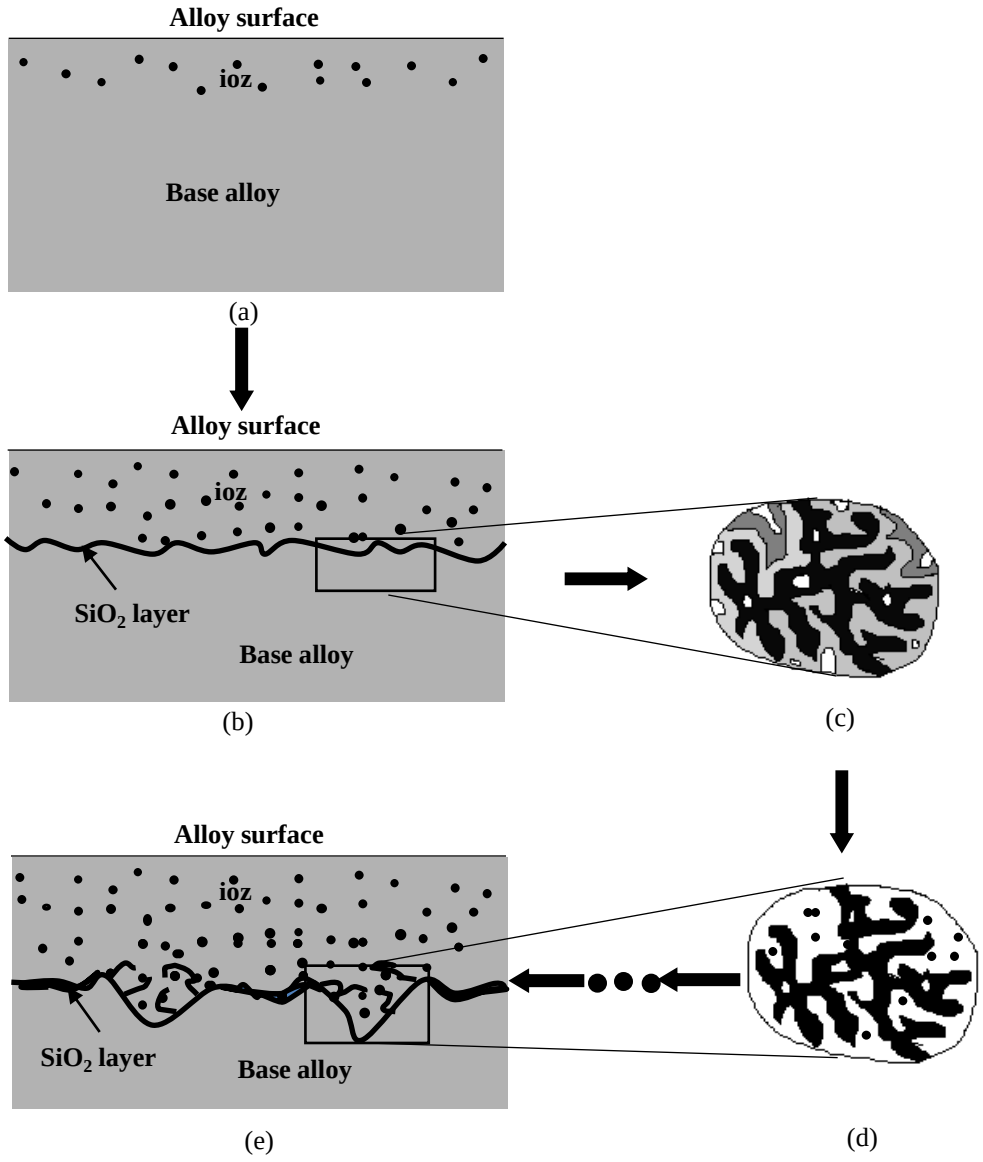

Fig.10 Schematics of the development of the anomalous ioz and the breakdown of the SiO_2 layer on Fe-5Si.

(a): Initial stage before the formation of the SiO_2 layer; (b): Formation of the SiO_2 layer; (c): Appearance of fissures in the SiO_2 layer viewed parallel to the layer; (d): Formation of the net-shaped and spherical SiO_2 viewed parallel to the layer; (e): Reformation of the SiO_2 layer.